Journal of Hazardous Materials 186 (2011) 1218–1225

Contents lists available at ScienceDirect

Journal of Hazardous Materials

journal homepage: www.elsevier.com/locate/jhazmat

Beta zeolite supported sol–gel TiO_2 materials for gas phase photocatalytic applications

Mama Lafjah[a,b], Fatiha Djafri[b], Abdelkader Bengueddach[b], Nicolas Keller[a], Valérie Keller[a,*]

[a] Laboratoire des Matériaux, Surfaces et Procédés pour la Catalyse (LMSPC), CNRS, University of Strasbourg, 25 rue Becquerel 67087, Strasbourg, France
[b] Laboratoire de Chimie des Matériaux (LCM), Université d'Oran, Es-senia, BP 15 24 El-Menouer, Oran, Algeria

ARTICLE INFO

Article history:
Received 29 September 2010
Received in revised form
28 November 2010
Accepted 30 November 2010
Available online 8 December 2010

Keywords:
Sol–gel TiO_2
Beta zeolite
Gas-phase photocatalysis
Methanol degradation
Supported photocatalyst

ABSTRACT

Beta zeolite supported sol–gel TiO_2 photocatalytic materials were prepared according to a sol–gel route in which high specific surface area Beta zeolite powder was incorporated into the titanium isopropoxide sol during the course of the sol–gel process. This led to an intimate contact between the zeolite surface and the TiO_2 precursors, and resulted in the anchorage of large amounts of dispersed TiO_2 nanoparticles and in the stabilization of TiO_2 in its anatase form, even for high TiO_2 wt. contents and high calcination temperatures. Taking the UV-A photocatalytic oxidation of methanol as gas phase target reaction, high methanol conversions were obtained on the Beta zeolite supported TiO_2 photocatalysts when compared to bulk sol–gel TiO_2, despite lower amounts of TiO_2 within the photoactive materials. The methanol conversion was optimum for about 40 wt.% TiO_2 loading and calcination temperatures of 500–600 °C.

1. Introduction

The Clean Air Act of 1990 has ruled the regulation of volatile organic compounds (VOCs) emitted by industrial processes, creating a strong incentive for research in this area in the last decades inside communities involved in innovative sustainable environmental research. More recently, the indoor air quality is receiving a growing interest due to the public concern over human health, and for which primarily VOCs are of concern [1,2]. Among filtration or newly developed advanced oxidation technologies, photocatalytic oxidation over UV-A light-activated wide band gap semiconductors is promising for removing contaminants from air at room temperature [1,3–5].

Among the used semiconductors, the wide band-gap TiO_2 is up to now the most attractive one with high photocatalytic efficiency under UV-A illumination [3–6]. Nevertheless, although commercial TiO_2 is a widespread UV-A photocatalyst for mineralizing pollutants in many environmental applications, its behaviour remains limited by photocharge recombination [7] and by adsorption–desorption behaviour of reactants and reaction products [8], so that the photocatalytic activity of TiO_2 is often not high enough to be used as-such for industrial purposes, while it cannot be used with visible-light illumination sources. Therefore, working at the material level for developing more efficient photocatalytic materials based on TiO_2 is of importance for sustainable development and for targeting viable processes. Among many approaches, adding adsorbents such as activated charcoal, alumina, silica or zeolite to TiO_2 has been reported to be an interesting way for increasing the process efficiency [9–11] and among them, zeolites have attracted an increasing interest due to a high surface area, hydrophobic/hydrophilic properties, easily tunable properties and a environmentally friendly nature [12,13]. In parallel to the design of highly dispersed Ti-oxide single-site catalysts within zeolite frameworks [14–16], TiO_2 nanoparticles and zeolite adsorbents have been efficiently associated by mechanical mixing with commercial crystallized TiO_2 nanoparticles [17–20], and scarcely by direct sol–gel synthesis of TiO_2 nanoparticles anchored at the zeolite surface [21], in both cases for liquid-phase photocatalytic oxidation reactions.

Mahalakshmi et al. evidenced the interest of using a mechanically mixed TiO_2-Beta zeolite composite compared to its bulk TiO_2 analogue for the aqueous liquid-phase propoxur degradation [12], the zeolite acting for gathering and concentrating the reactant and the intermediates within the framework cavities and further supplying them on the neighbouring TiO_2 surfaces, resulting in the enhancement of reaction and mineralization rates. In addition, they have reported that the Beta zeolite was a better support for TiO_2 than Y and ZSM-5 zeolites due to a greater adsorption capacity towards propoxur as well as towards hydrophilic reaction intermediates. Shankar et al. have also reported that

* Corresponding author. Tel.: +33 36885 736; fax: +33 36885 761.
E-mail address: vkeller@chimie.u-strasbg.fr (V. Keller).

0304-3894/$ – see front matter © 2010 Elsevier B.V. All rights reserved.
doi:10.1016/j.jhazmat.2010.11.134

the enhanced adsorption properties shown by the Beta zeolite supported TiO_2 materials compared to bulk TiO_2 increased the photocatalytic degradation of monocrotophos pesticide, a TiO_2 content of 3 wt.% being enough to get a higher degradation rate together with a shorter duration required for complete mineralization of the inlet carbon [18]. One should also note that Reddy et al. observed that TiO_2-loaded Beta zeolite was not active for the salicylic acid because of its low hydrophilicity, while it was very active towards the formic acid [17]. Similarly to the mineralization of organic chemical molecules, Beta zeolite was also reported to concentrate the bacteria during the photocatalytic disinfection of *Escherichia coli* bacteria-contaminated water [19]. The authors also highlighted that the surface charges of the zeolite could favour the high mechanical adsorption/adhesion of negatively charged Gram-negative bacteria cells.

Given the objective of overcoming the limitations of commercial TiO_2, emphasis has been put on the tunable and versatile sol–gel synthesis routes, which are highly promising for (i) improving the efficiency of TiO_2-based photocatalysts, (ii) tuning the materials as a function of the molecule to degrade or of the activation source for transferring the activation to the visible range, or (iii) preparing high transparency thin films for surface applications [22–26]. Preparing zeolite supported TiO_2 photocatalysts through sol–gel procedures remained however scarcely reported for directly anchoring TiO_2 nanoparticles at the zeolite surface [21]. The aim of this paper is thus to report on the vapor phase use of Beta zeolite supported TiO_2 nanoparticle photocatalytic materials prepared by the sol–gel route, taking the UV-A photocatalytic oxidation of methanol as gas-phase target reaction.

2. Experimental

2.1. Catalyst preparation

The bare Beta zeolite was synthesized according to a three step synthesis process. First, the synthesis consisted in preparing the amorphous SiO_2–Al_2O_3 mixed oxides used as raw materials following a two step sol–gel method. Tetraethylorthosilicate (TEOS, Aldrich) was first prehydrolysed at room temperature in an acidic medium before adding $Al(NO_3)_3{\cdot}9H_2O$ aluminium nitrates (Prolabo) as aluminium source. The mixture was then cooled down to 0 °C before a solution of tetra-*n*-butyl orthotitanate (TBOT, Merck) in isopropanol was added dropwise under stirring. The cogel was further obtained by adding tetraethylammonium hydroxide (TEAOH, Aldrich) to this mother solution, in order to accelerate the gelation process. After drying of the cogel at 100 °C for 12 h and further grinding to get a white powdered material, the second step consisted in the wetness impregnation of the obtained xerogel by a 35% TEAOH aqueous solution as organic templating agent. The impregnated xerogel was subsequently hydrothermally treated in a Teflon-lined autoclave (200 mL) at 150 °C under autogeneous pressure for 7 days. Afterwards, the filtred solid phase was washed several times with demineralized water till neutral pH before being dried overnight at 60 °C. Final calcination of the material was performed in air at 550 °C for 6 h with a heating rate of 20 °C/min for removing the templating agent.

The bulk TiO_2 synthesis was performed by a sol–gel procedure in which the $Ti[OCH(CH_3)_2]_4$ titanium isopropoxide precursor (TIP, Fluka) was put together with water and ethanol at a basic pH (rectified at 9 by dropwise addition of ammonia) for 1 h under stirring. The solid was filtred, washed with flowing ethanol, before being washed again in an ethanol solution under stirring and finaly filtred. This sequence was triplicated. Drying was performed overnight at 80 °C before calcination in air for 2 h at temperatures ranging from 420 °C to 800 °C.

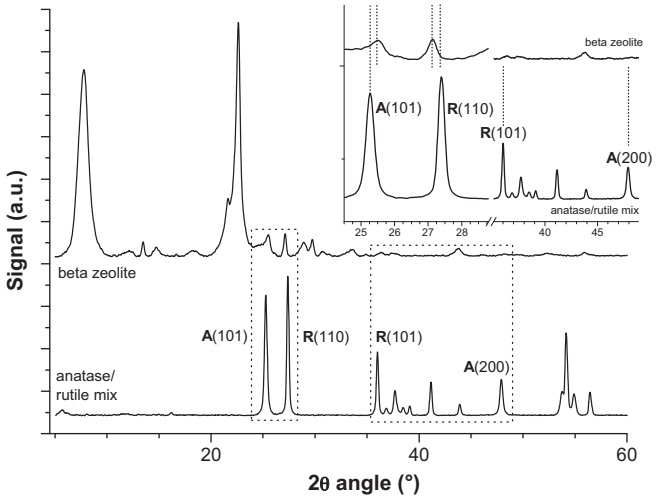

Fig. 1. Powder XRD pattern of the bare Beta zeolite and of a sol–gel TiO_2 obtained for a calcination temperature of 600 °C, evidencing both anatase and rutile TiO_2 phases. Inlet: zoom on the 24–29° and 35–49° ranges in 2θ.

The Beta zeolite supported TiO_2 photocatalytic materials were synthesized by performing the sol–gel procedure as described above, in the presence of previously synthesized Beta zeolite powder, with TiO_2 wt. contents ranging from 3.8 wt.% to about 50 wt.%. The zeolite powder was incorporated to the TIP/ethanol mixture and kept under stirring for 1 h, before water for the hydrolysis step and further ammonia for rectifing the pH to 9 were added. Filtration and drying were subsequently performed as for the zeolite-free sol–gel material, and the resulting materials were finally calcined in air for 2 h at temperatures ranging from 420 °C to 800 °C to get the TiO_2/zeolite photocatalysts. The TiO_2 wt. content was defined as the weight of TiO_2 relative to the weight of the photocatalytic material, the bulk sol–gel TiO_2 reference corresponding to a 100 wt.% TiO_2 content.

2.2. Characterization techniques

X-ray diffraction (XRD) measurements were carried out on a D8 Advance Bruker diffractometer in a $\theta/2\theta$ mode and using the Kα_1 radiation of Cu at 1.5406 Å. Fig. 1 shows the XRD diagrams of the Beta zeolite and of a typical anatase/rutile TiO_2 mixed system, for evidencing that some diffraction peaks of the Beta zeolite could interfer with the most intense diffraction peaks of both rutile and anatase phases, *i.e.* the (1 1 0) and (1 0 1) peaks at 27.4° and 25.3°, respectively, according to the JCPDS files No. 21-1276 and 21-1272, respectively. Therefore, the content and the mean crystallite size of both rutile and anatase phases were mainly determined from diffraction peak intensities of the (1 0 1) plane at 36.1° for the rutile phase, and of the (2 0 0) plane at 48.1° for the anatase phase. Care has been taken that the choice of the diffraction peak did not influence the results, by comparing the mean crystallite sizes obtained on highly loaded zeolites, for which the possibly interferring diffraction peaks of the zeolite were considered as negligeable.

The surface area and porosimetry measurements were carried out on a ASAP2010 Micromeritics using N_2 as adsorbant at liquid N_2 temperature. Before the N_2 adsorption, the material was outgassed at 200 °C for 3 h in order to desorb the impurities or moisture from its surface. The total surface area was calculated from the N_2 adsorption isotherms using the BET method and the micropore surface area was derived from the *t*-plot curve.

Table 1
Specific surface area with microporous content, TiO_2 anatase/rutile ratio and TiO_2 mean particle size as a function of the calcination temperature, for bulk sol–gel TiO_2 and TiO_2/Beta zeolite materials.

	TiO_2 content (in wt.%)							
	3.8%	11.4%	13.7%	17.5%	24.3%	39.2%	49.2%	Bulk TiO_2
420 °C								
BET area (m^2/g) [micropores in m^2/g]	509 [445]	499 [414]	484 [401]	457 [395]	–	–	–	31 [0]
Anatase/rutile (%/%)	[a]	100/0	100/0	100/0	–	–	–	100/0
Mean anatase particle size	[a]	[a]	[a]	[a]	–	–	–	9
500 °C								
BET area (m^2/g) [micropores in m^2/g]	538 [359]	437 [311]	458 [320]	457 [280]	429 [306]	384 [214]	313 [149]	20 [0]
Anatase/rutile (%/%)	[a]	100/0	100/0	100/0	100/0	100/0	100/0	89/11
Mean anatase particle size	[a]	16	11	10	10	9	8	16 (Rutile: 24)
600 °C								
BET area (m^2/g) [micropores in m^2/g]	533 [357]	422 [295]	429 [298]	423 [259]	416 [298]	338 [199]	287 [133]	10 [0]
Anatase/rutile (%/%)	[a]	100/0	100/0	100/0	100/0	100/0	100/0	52/48
Mean anatase particle size	[a]	14	9	7	11	10	10	33 (Rutile: 40)
700 °C								
BET area (m^2/g) [micropores in m^2/g]	501 [342]	463 [326]	356 [253]	432 [275]	362 [241]	308 [179]	269 [148]	8 [0]
Anatase/rutile (%/%)	[a]	100/0	100/0	100/0	100/0	100/0	100/0	23/77
Mean anatase particle size	[a]	15	12	9	12	11	10	36 (Rutile: 44)
800 °C								
BET area (m^2/g) [micropores in m^2/g]	416 [346]	384 [327]	423 [365]	475 [309]	–	–	–	6 [0]
Anatase/rutile (%/%)	[a]	100/0	100/0	100/0	–	–	–	0/100
Mean anatase particle size	[a]	11	10	10	–	–	–	(Rutile: 53)

[a] Non-measurable due to the low amount of TiO_2 in the samples and/or the lack in crystallinity.

2.3. Experimental device and procedure

The photocatalytic reaction was carried out in a 260 mm length single pass annular Pyrex reactor made of two coaxial tubes 3 mm apart, between which the reactant mixture was passing through. Extensive details concerning both photocatalytic reactor and device can be found elsewhere [27]. An adequate amount of photocatalytic material was evenly coated on the internal side of the 28 mm *i.d.* external tube by evaporating a catalyst-containing aqueous slurry to dryness. Most of the efficiency tests were performed with 420 mg of photocatalytic material deposited inside the reactor, corresponding to a coverage density (*i.e.* a TiO_2 reactor coverage) of 0.87 mg/cm^2. The catalyst coated reactor was finally dried at 110 °C for 1 h in air. Methanol (Fluka, >99.8%) was fed at atmospheric pressure by bubbling air through a temperature-controlled saturator, and mixed with additional air, both regulated by mass-flow controllers, to obtain a methanol concentration of 1400 vol. ppm at the required constant total air flow. Before the photocatalytic reaction, the catalyst was first exposed to the polluted air stream with no illumination until dark-adsorption equilibrium was reached. Afterwards the UV-A illumination was switched on. Illumination was provided by a commercially available 8W black light tube (Philips, TL8W/08 BLB F8T5, 3.8 mW cm^{-2} of irradiance) with a spectral peak centered on 365 nm, located inside the inner tube of the reactor. The reaction was then performed at total flow rates of 550 mL/min and 2 L/min with gas velocities of 3.9 cm/s and 14.1 cm/s, respectively, corresponding to residence times of 6.7 s and 1.8 s, and to vapor hourly space velocities of 540 h^{-1} and 1960 h^{-1}, respectively.

The photocatalytic performances were obtained by *on-line* analyzing and quantifying both inlet and outlet flows with a microgas chromatography (Agilent 3000, SRA-Instruments) through OV1 and PPQ columns coupled to thermal conductivity detectors.

3. Results and discussion

3.1. Material characterization

Table 1 summarizes the BET specific surface area with microporous content derived from the *t*-plot method, the anatase/rutile TiO_2 ratio and the TiO_2 mean particle size for the bulk sol–gel TiO_2 and the TiO_2/Beta zeolite materials. Fig. 1 shows the powder XRD diagram of the bare zeolite shown in Fig. 1 confirmed the crystallization of the Beta zeolite in the BEA structure. Fig. 2(A)–(E) compared the powder XRD patterns of bulk sol–gel TiO_2 and of TiO_2/Beta zeolite materials at different TiO_2 contents obtained for calcination temperatures ranging from 420 °C to 800 °C. As expected, the crystalline nature of bulk sol–gel TiO_2 materials progressively turned with increasing the calcination temperature, from pure anatase at 420 °C into pure rutile at 800 °C, together with a decrease in specific surface area from 31 m^2 g^{-1} to 6 m^2 g^{-1} and an increase in the TiO_2 crystallite mean size from 9 nm up to about 50 nm. By contrast, the diffraction patterns of the zeolite supported TiO_2 materials did not show the presence of any rutile TiO_2 phase, with no diffraction peaks assigned to the rutile phase being observed, whereas the anatase phase was the sole TiO_2 phase to be observed whatever the TiO_2 wt. content and the calcination temperature. In addition to that, it was worth noting that the anatase mean size remained approximatively unchanged, around 11 ± 2 nm, whatever the TiO_2 wt. content up to 49.2 wt.% and the calcination temperature up to 800 °C.

The reference bare zeolite had a specific surface area of 644 m^2 g^{-1} with a microporous content of 533 m^2 g^{-1}. As a function of the TiO_2 wt. content, the synthesis of sol–gel TiO_2 on the Beta zeolite led to a decrease in the specific surface area, *e.g.* for a calcination temperature of 600 °C, down to 533 m^2 g^{-1} and 287 m^2 g^{-1} for 3.8 wt.% and 49.2 wt.% contents, respectively. However, whatever the TiO_2 wt. content, the N_2 adsorption–desorption isotherms shown in Fig. 3 for samples calcined at 600 °C, remained characteristic of materials with a high microporous fraction, and with the hysteresis branch being representative of the presence of intercrystalline mesopores resulting from the agglomeration of small size crystallites.

The different characterizations evidenced that the presence of the zeolite support during the sol–gel synthesis avoided the sintering of the TiO_2 particles, even for high calcination temperatures up to 800 °C and even up to TiO_2 wt. contents of 49.2 wt.%. Indeed, one could expect that for so high TiO_2 loadings, the synthesized material would not been influenced by the presence of the zeolite material and consequently would display the properties of bulk sol–gel TiO_2, *i.e.* appearance of rutile phase and particle sintering with increasing the calcination temperature. The TiO_2/Beta zeolite materials could

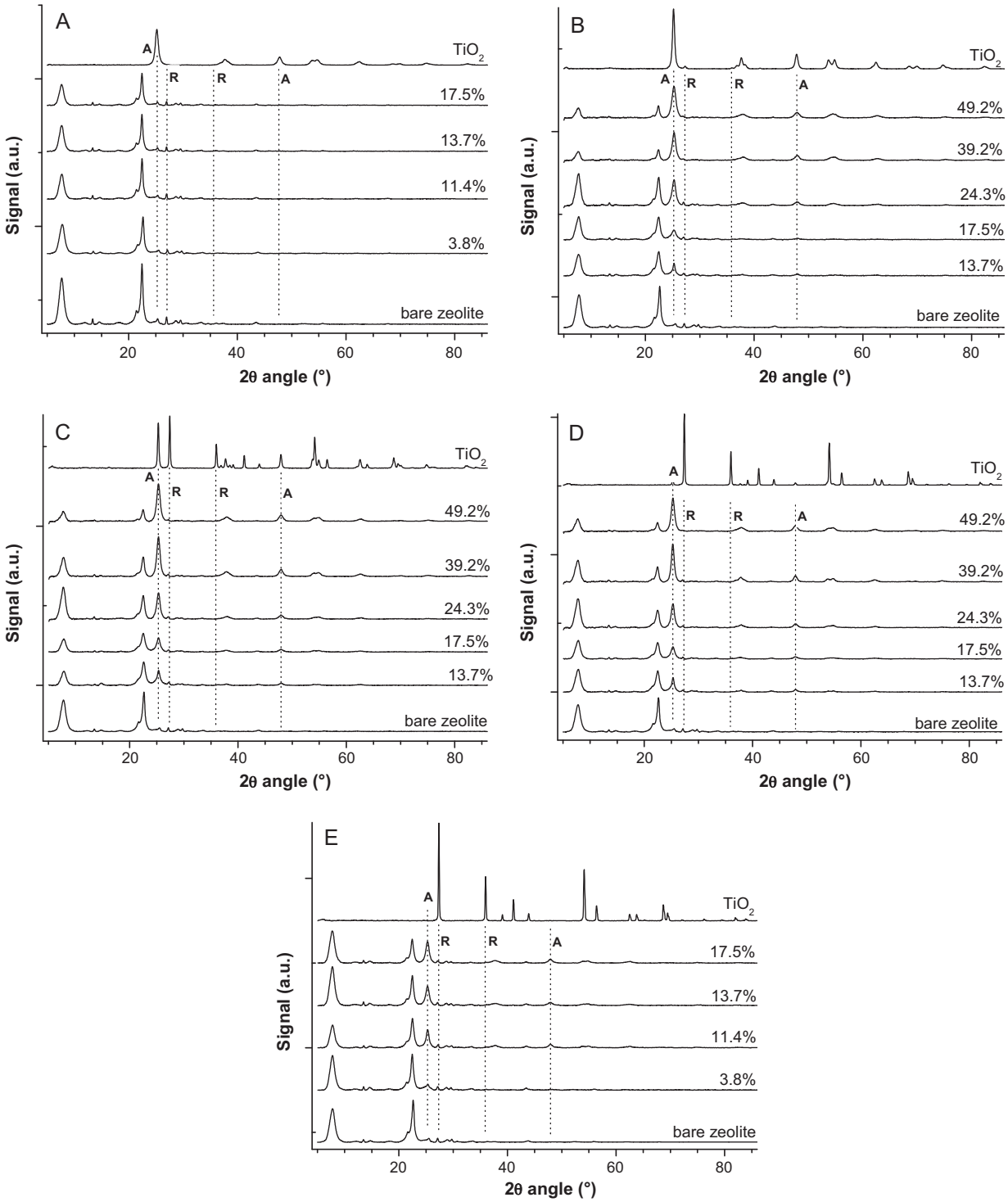

Fig. 2. Powder XRD pattern of the bare Beta zeolite, the sol–gel TiO_2 and the TiO_2/Beta zeolite materials at different TiO_2 wt. contents in the 3.8–49.2 wt.% range, obtained for calcination temperatures of (A) 420 °C, (B) 500 °C, (C) 600 °C, (D) 700 °C and (E) 800 °C. Samples calcined at 420 °C and 800 °C have not been prepared with more than 17.5 wt.% of TiO_2 according to the preliminary study results. A and R labels corresponded to diffraction angles for anatase and rutile phases, respectively.

thus be considered as Beta zeolite decorated by TiO_2 nanoparticles, even for a very high TiO_2 wt. content.

The role played by the Beta zeolite material incorporated during the sol–gel synthesis procedure could probably result from the high surface area of the support material. It allowed the grafting and the anchorage, firstly of the titanium-based sol and further of the amorphous $Ti(OH)_4$-based precursor units, that hindered the growing of the anchored nanoparticles. This strongly contrasted with the sintering observed during the synthesis of bulk TiO_2, resulting simultaneously in larger TiO_2 particles and in the appearance of the rutile phase for a calcination temperature of 500 °C, and becoming the main crystallized TiO_2 phase for calcination temperatures higher than 600 °C.

The interaction between the zeolite support surface and the TiO_2 precursor species could play a similar role than that occurring during template- or porogen-assisted syntheses of sol–gel TiO_2, in which the influence of the functional groups of the incorporated molecules has been pointed out during the hydrolysis step of

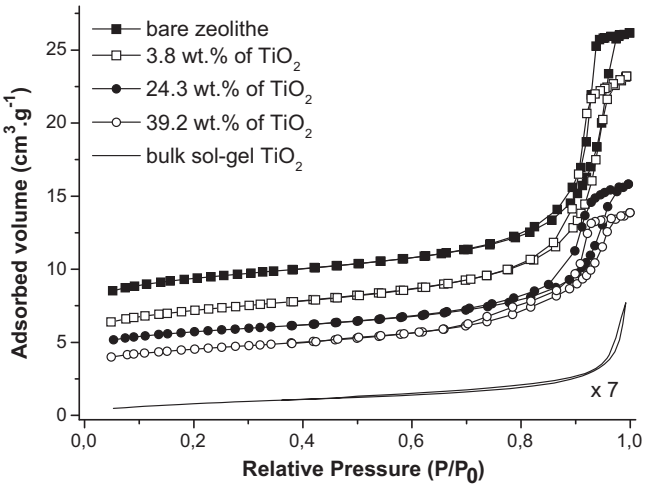

Fig. 3. Nitrogen adsorption–desorption isotherms of the bare Beta zeolite, the sol–gel TiO_2 (7 times zoomed) and the TiO_2/Beta zeolite materials at different TiO_2 contents, calcined at 600 °C.

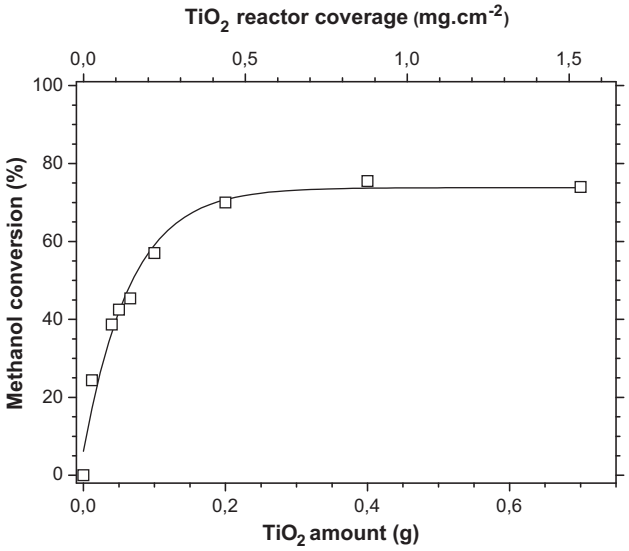

Fig. 4. Methanol conversion obtained at a flow rate of 550 mL/min on the bulk sol–gel TiO_2 calcined at 600 °C, as a function of the amount of TiO_2-coated on the reactor wall (expressed also in top-axis as the TiO_2 reactor wall coverage in mg cm^{-2}).

the synthesis [28]. The surface polarity could lead to strong interactions between the growing titania particles in formation into the sol–gel and the surface groups of the Beta zeolite. Those latter could act in place of and on a similar way than the functional groups of templating/porogen molecular agents, for which hydrogen bond formation between templating agents and the growing titania particles in formation have already been evidenced using IR spectroscopy. It was also already reported that the anatase-to-rutile ratio of unsupported sol–gel TiO_2 materials was strongly influenced by the nature of the templating or porogen molecules [29]. The interaction between TiO_2 precursor species and organic molecules at different steps of the sol–gel procedure, was also already used for designing protecting-group syntheses, in which the organic molecules were playing a role of crystallite growth inhibitor, resulting in the synthesis of nanosized TiO_2 [30–33]. In this synthesis, the replacement of the –OH groups in the titanium-containing gel by hexamethyldisilazane $[Si(CH_3)_3(NH)_2]$ to form methyl siloxyl $[-OSi(CH_3)_3]$ surface groups inhibited the crystallite growth and led to the synthesis of few nm mean size TiO_2 nanoparticles. This was attributed to the non-condensing character of the methyl siloxyl surface groups, in comparison to that of the –OH groups prone to condense during calcination.

3.2. Photocatalytic results

The vapour phase oxidation of methanol has been taken as target reaction for evaluating the efficiency of the TiO_2-based photocatalytic materials. Fig. 4 shows the methanol conversion obtained at a flow rate of 550 mL/min on the sol–gel TiO_2 calcined at 600 °C, as a function of the amount of TiO_2 coated on the reactor wall (expressed also in top-axis as the TiO_2 reactor coverage in mg cm^{-2}).

No significant methanol adsorption was measured on the TiO_2 coated glass reactor and it should be noted that no methanol oxidation occurred with the sole UV-A irradiation in the absence of TiO_2. Performing the methanol oxidation in the TiO_2-coated annular photoreactor led to a photocatalytic behaviour as a function of the TiO_2 content (*i.e.* the reactor coverage) in agreement with the usual pattern as reported in the literature [34]. The photocatalytic activity first rapidly increased with increasing the TiO_2 amount, due to the increase in the amount of TiO_2 in which all the particles, *i.e.* all the surface exposed – are totally illuminated, before developing into conversion levels around 75%. This conversion plateau was reached for an optimal surface coverage value of about 0.87 mg cm^{-2}, corresponding to a TiO_2 reactor content of 0.4 g for a 28 mm *i.d.* annular photoreactor. For higher amounts of catalyst (*i.e.* larger surface coverages), a screening effect of excess particles occurs, which masks part of the photosensitive semiconductor particles, due to the limited penetration thickness of UV-A illumination, and the methanol remained unchanged as expected. According to that, performing the further evaluation of the photocatalytic materials at a surface coverage of 0.87 mg cm^{-2} will ensure the activation of the whole photocatalyst, whatever its chemical composition, *i.e.* for both bulk sol–gel TiO_2 and zeolite supported sol–gel TiO_2 photocatalysts.

Fig. 5 shows the methanol conversion obtained at a flow rate of 550 mL/min on the TiO_2 (3.8–17.5 wt.%)/Beta zeolite photocatalysts and on the bulk sol–gel TiO_2, calcined at a temperature in the 420–800 °C range (at a 0.87 mg cm^{-2} reactor coverage). The methanol conversion obtained on the bulk sol–gel TiO_2 regularly decreased with increasing the calcination temperature, from 92% at 420 °C down to 62% for a calcination temperature of 800 °C. The expected behaviour of the bulk sol–gel TiO_2 was attributed to (i) the decrease in its specific surface area with increasing the thermal

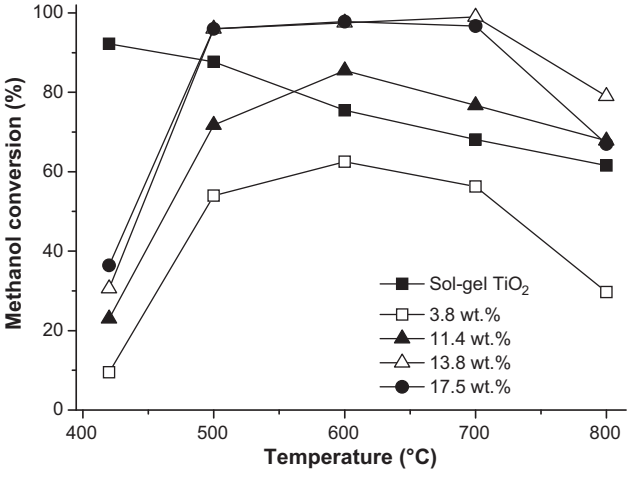

Fig. 5. Methanol conversion obtained at a flow rate of 550 mL/min on the TiO_2 (3.8–17.5 wt.%)/Beta zeolite photocatalysts and on the bulk sol–gel TiO_2, calcined at temperatures in the 420–800 °C range (at a 0.87 mg cm^{-2} reactor coverage).

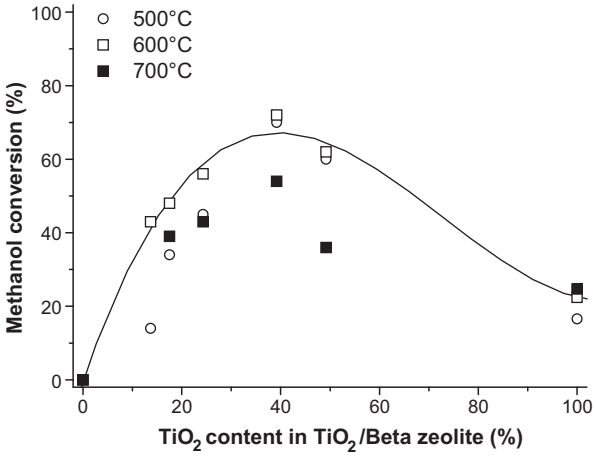

Fig. 6. Methanol conversion obtained on the Beta zeolite supported sol–gel TiO_2 photocatalytic materials calcined at temperatures between 500 °C and 700 °C with different TiO_2 contents up to 49.2 wt.%, at a flowrate of 2 L/min (at a 0.87 mg cm^{-2} reactor coverage). The 100 wt.% TiO_2 sample corresponded to bulk sol–gel TiO_2.

treatment temperature, from 31 m^2 g^{-1} down to 6 m^2 g^{-1} for a temperature of 800 °C, with a simultaneous increase in the crystallite size, resulting in a decrease in the adsorption capacity of the sol–gel TiO_2 particles, and (ii) the temperature-activated structural phase change from pure anatase to pure rutile TiO_2 with lower activity for a calcination temperature of 800 °C. One could note that the gain in TiO_2 crystallinity resulting from a higher calcination temperature was not large enough for overcoming the above mentioned detrimental phenomena, as well as the possible coupling between the anatase and rutile phases within mixed TiO_2 systems – if occuring here – often reported to be beneficial for limiting the photogenerated charge recombination in case of mixed anatase/rutile systems with adequate relative contents [33,35].

By contrast, whatever the sol–gel TiO_2 content of the zeolite-based photocatalysts, the methanol conversion curve displayed a volcano-like pattern, with a maximum of conversion being obtained for calcination temperatures ranged between 500 °C and 700 °C. In addition to that, higher the TiO_2 content supported on the zeolite, higher the methanol conversion. As a result, one could note that the high methanol conversions near values of 100% obtained for samples calcined at temperatures in the 500–700 °C range and with TiO_2 contents higher than 13.8 wt.%, did not allow to discriminate between those photocatalysts.

Therefore, this preliminary study highlighted the interest of investigating the influence of the TiO_2 wt. content in the zeolite supported sol–gel TiO_2 photocatalytic materials calcined at temperatures between 500 °C and 700 °C, on the methanol conversion obtained at a flow rate of 2 L/min and at a 0.87 mg cm^{-2} reactor coverage, as shown in Fig. 6. It was worth noting that, whatever the calcination temperature between 500 °C and 700 °C, the methanol conversion curve displayed a similar volcano-like pattern with increasing the sol–gel TiO_2 content of the zeolite-based photocatalysts, with maxima of methanol conversion being observed for TiO_2 contents of about 50 wt.% for all samples. For samples calcined at 500 °C, the methanol conversion increased up to 70% with increasing the TiO_2 content up to 39.2 wt.%, whereas it decreased down to 17% for the bulk sol–gel TiO_2 reference. A similar behaviour was shown for samples calcined at 600 °C, for which a maximum of methanol conversion of 72% was recorded at a TiO_2 content of 39.2 wt.%, a conversion of 22% being observed for the bulk TiO_2 material. The material calcined at 700 °C displayed a less marked behaviour, with an increase in the methanol conversion up to 54% for a TiO_2 content of 39.2 wt.% and a decrease in the methanol conversion down to 25% on the bulk sol–gel TiO_2 sample.

Similar volcano curves have been already reported in previous works performed in liquid-phase on Beta zeolite supported TiO_2 photocatalysts obtained by direct mechanical blending of commercial TiO_2 powder with zeolite. Indeed, Mahalakshmi et al. have observed that the increase in the amount of TiO_2 on the Beta zeolite increased the propoxur degradation rate up to 7 wt.% whereas it strongly decreased for higher TiO_2 contents [12]. The authors attributed this decrease to less adsorption of propoxur and to light scattering effect. In addition, they hypothesized the absence at high loadings of any intimate contact between the TiO_2 particles and the zeolite, leading to the absence of any electron transfer from the excited TiO_2 conduction band to the zeolite framework, and resulting in the absence of any electron–hole recombination limitation. Similar results were obtained by Shankar et al. in the slurry-batch degradation of the monocrotophos pesticide, with an optimum rate at a 3 wt.% TiO_2 content relatively to the Beta zeolite support [18]. The blending of commercial TiO_2 particles with siliceous mordenite zeolite was also reported by Takeuchi to display an optimum in the mineralization yield of gaseous acetaldehyde within the 2.5–15 wt.% range [20]. They attributed this behaviour with decreasing the mordenite zeolite content, to the fact that a too low zeolite content was not efficient enough for gathering the gaseous acetaldehyde molecules within the hydrophobic zeolite cavities for further supplying them onto the photocatalytically active TiO_2 surface. They also reported that the wider plateau of optimum conversion (up to 15 wt.% TiO_2 loadings) compared to other works, was attributed to the high transparency of the siliceous zeolite powder, which allowed the whole part of the TiO_2 particles to be sufficiently irradiated inside the TiO_2/zeolite material coating.

It was worth noting that, in contrary to materials prepared with already crystallized TiO_2 particles, directly anchoring and synthesizing the TiO_2 nanoparticles onto the zeolite surface allowed a shift in the TiO_2 optimum content towards higher loadings to be achieved, the maximum of methanol conversion being obtained for TiO_2 contents of about 50 wt.% whatever the sample calcination temperature. It should be noted that no significant differences in terms of absorption edges as a function of the TiO_2 wt.% content in TiO_2/Beta zeolite materials was observed (Supplementary Material), so that it could not be proposed for explaining the reactivity volcano curve as a function of the TiO_2 wt.% content.

The hypothesis of a partial illumination of the sol–gel TiO_2 coating within the annular reactor, that would lead to underestimated the activity per mass of TiO_2, was mainly ruled out by the absence of any screening effect at a surface coverage of 0.87 mg cm^{-2}, as shown in Fig. 4, that ensures the activation of the whole sol–gel TiO_2 photocatalytic coating. Thus, the possibility to achieve high methanol conversions on the Beta zeolite supported TiO_2 photocatalysts when compared to bulk sol–gel TiO_2, despite strongly lower amounts of TiO_2 within the photoactive materials was attributed to:

(i) The stabilisation of anatase TiO_2 nanoparticles anchored at the surface of the Beta zeolite with intimate contact between the active particles and the adsorbent support.
(ii) The artificial increase of the residence time of the methanol reactant molecules within the photocatalytic material and close to the active TiO_2 nanoparticles, due to the presence of the highly adsorbent zeolite crystallites. This is in relation with the 'Adsorb and Shuttle' concept, in which the inert domains of the zeolite adsorbent are used for adsorbing the pollutant before releasing to the neightbouring photocatalytic sites. Activated carbon was one of the first adsorbent materials for which this concept was demonstrated [36,37], before the concept was extended to silica, alumina or zeolites [38–40].
(iii) The *on-stream* continuous regeneration of the adsorption sites of the zeolite, due to the intimate contact between both

adsorption and photocatalytic sites. This regeneration was proposed to occur through the 'Remote Degradation' mechanism, based on the surface diffusion of active oxiding chemical species from the TiO_2, where they are formed, to the adsorbent sites on which the pollutants are adsorbed [41–43]. Diffusion lengths up to 80 μm have already been observed, and this mechanism was first mentioned for the liquid phase photodegradation of rhodamine 6G on microdomains-based silica–titania mixed composite particles [36].

One could also note that achieving a high TiO_2 dispersion at high TiO_2 wt.% content when directly grafting the TiO_2 nanoparticles during the synthesis, should allow an intimate contact between the active TiO_2 nanoparticles and the zeolite surface to be maintained. Therefore, in contrast to the TiO_2 and zeolite mechanical mixing, this intimate contact between the Beta zeolite and the supported TiO_2 could allow the transfer of the excited electrons from the TiO_2 conduction band to the zeolite surface to be effective, and thus the electron–hole recombination rate to be decreased, as previously put forward by Mahalakshmi et al. [12] and Shankar et al. [18].

4. Conclusions

This article reports on the use of Beta zeolite supported TiO_2 photocatalytic materials for gas phase photocatalytic applications, taking the UV-A photocatalytic oxidation of methanol as target reaction. Efficient Beta zeolite supported TiO_2 photocatalysts were prepared through an easily tunable sol–gel procedure by incorporating Beta zeolite powder into the TIP-based sol. High methanol conversions have been achieved on the Beta zeolite supported TiO_2 photocatalysts when compared to bulk sol–gel TiO_2, despite lower amounts of TiO_2 within the photoactive materials. The conversion pattern followed a volcano-like curve as a function of the TiO_2 wt.% and of the calcination temperature, with an optimum in efficiency being obtained for a 39.2 wt.% TiO_2 loading and calcination temperatures of 500–600 °C. The sol–gel synthesis procedure and the high surface area of the Beta zeolite material allowed an intimate contact between the zeolite surface and the TiO_2 precursors to be achieved resulting in the anchorage of large amounts of dispersed TiO_2 nanoparticles and in the maintain of TiO_2 in its anatase form, even for high TiO_2 wt. contents and high calcination temperatures. The stabilisation of the anatase form, the artificial increase of the residence time of methanol within the photocatalytic material and close to TiO_2, the continuous regeneration of the zeolite sites due to the intimate contact between adsorption and active sites and the enhanced transfer of TiO_2 excited electrons to the zeolite, leading to decrease the recombination rate, were put forward for explaining the improved photocatalytic efficiency.

Acknowledgements

The authors thank the Algerian Ministry for Higher Education and the French Ambassy in Alger for providing a PhD grant to Mama Lafjah through the frame of the PROFAS (Programme franco-algérien de formation supérieure en France).

Appendix A. Supplementary data

Supplementary data associated with this article can be found, in the online version, at doi:10.1016/j.jhazmat.2010.11.134.

References

[1] S. Romero-Vargas Castrillon, H.I. de Lasa, Performance evaluation of photocatalytic reactors for air purification using computational fluid dynamics (CFD), Ind. Eng. Chem. Res. 46 (2007) 5867–5880.
[2] B. Lomborj, The Skeptical Environmentalist, Cambridge University Press, Cambridge, UK, 2001.
[3] D.F. Ollis, E. Pelizzetti, N. Serpone, Destruction of water contaminants, Environ. Sci. Technol. 25 (1991) 1522–1529.
[4] M. Schiavello (Ed.), Photocatalysis and Environment. Trends and Applications, Kluwer-Academic Publishers, Dordrecht, 1988.
[5] E. Pelizzetti, N. Serpone (Eds.), Photocatalysis. Fundamentals and Applications, Wiley, New York, 1989.
[6] D.F. Ollis, H. Al-Ekabi (Eds.), Photocatalytic Purification and Treatment of Water and Air, Elsevier, Amsterdam, 1993.
[7] B.J. Liu, T. Torimoto, H. Yoneyama, Photocatalytic reduction of CO, using surface-modified CdS photocatalysts in organic solvents, J. Photochem. Photobiol. A: Chem. 113 (1998) 93–97.
[8] J.A. Navio, G. Colon, J.M. Herrmann, Photoconductive and photocatalytic properties of $ZrTiO_4$. Comparison with the parent oxides TiO_2 and ZrO_2, J. Photochem. Photobiol. A: Chem. 108 (1997) 179–185.
[9] N. Takeda, T. Torimoto, S. Sampath, S. Kuwabata, H. Yoneyama, Effect of inert supports for titanium dioxide loading on enhancement of photodecomposition rate of gaseous propionaldehyde, J. Phys. Chem. 99 (24) (1995) 9986–9991.
[10] C. Anderson, A. Bard, Improved photocatalytic activity and characterization of mixed TiO_2/SiO_2 and TiO_2/Al_2O_3 materials, J. Phys. Chem. B 101 (14) (1997) 2611–2616.
[11] J. Matos, J. Laine, J.-M. Herrmann, Synergy effect in the photocatalytic degradation of phenol on a suspended mixture of titania and activated carbon, Appl. Catal. B: Environ. 18 (1998) 281–291.
[12] M. Mahalakshmi, S. Vishnu Priya, B. Arabindoo, M. Palanichamy, V. Murugesan, Photocatalytic degradation of aqueous propoxur solution using TiO_2 and Hβ zeolite-supported TiO_2, J. Hazard. Mater. 161 (2009) 336–343.
[13] A. Corma, From microporous to mesoporous molecular sieve materials and their use in catalysis, Chem. Rev. 97 (6) (1997) 2373–2420.
[14] J. Zhang, M. Minagawa, M. Matsuoka, H. Yamashita, M. Anpo, Photocatalytic decomposition of NO on Ti-HMS mesoporous zeolite catalysts, Catal. Lett. 66 (2000) 241–247.
[15] M. Takeuchi, S. Sakai, A. Ebrahimi, M. Matsuoka, M. Anpo, Investigations on the development of highly active titanium oxide photocatalysts and their reactivity for the oxidation of organic compounds, Top. Catal. 52 (2009) 1651–1659.
[16] M. Anpo, T.-H. Kim, M. Matsuoka, The design of Ti-, V-, Cr-oxide single-site catalysts within zeolite frameworks and their photocatalytic reactivity for the decomposition of undesirable molecules—the role of their excited states and reaction mechanisms, Catal. Today 142 (2009) 114–124.
[17] E.P. Reddy, L. Davydov, P. Smirniotis, TiO_2-loaded zeolites and mesoporous materials in the sonophotocatalytic decomposition of aqueous organic pollutants: the role of the support, Appl. Catal. B: Environ. 42 (11) (2003) 1–11.
[18] M.V. Shankar, K.K. Cheralathan, B. Arabindoo, M. Palanichamy, V. Murugesan, Enhanced photocatalytic activity for the destruction of monocrotophos pesticide by TiO_2/Hβ, J. Mol. Catal. A: Chem. 223 (2004) 195–200.
[19] M.P. Reddy, H.H. Phil, M. Subrahmanyam, Photocatalytic disinfection of escherichia coli over titanium (IV) oxide supported on Hβ zeolite, Catal. Lett. 123 (2008) 56–64.
[20] M. Takeuchi, J. Deguchi, M. Hidaka, S. Sakai, K. Woo, P.-P. Choi, J.-K. Park, M. Anpo, Enhancement of the photocatalytic reactivity of TiO_2 nano-particles by a simple mechanical blending with hydrophobic mordenite (MOR) zeolite, Appl. Catal. B: Environ. 89 (2009) 406–410.
[21] J. Chen, L. Eberlein, C.H. Langford, Pathways of phenol and benzene photooxidation using TiO_2 supported on a zeolite, J. Photochem. Photobiol. A: Chem. 148 (2002) 183–189.
[22] S. Sakthivel, H. Kisch, Daylight photocatalysis by carbon-modified titanium dioxide, Angew. Chem. Int. Ed. 42 (2003) 4908–4911.
[23] R. Asahi, T. Morikawa, T. Ohwaki, A. Aoki, Y. Taga, Visible-light photocatalysis in nitrogen-doped titanium oxides, Science 293 (2001) 269–271.
[24] S. Sakthivel, M. Janczarek, H. Kisch, Visible light activity and photoelectrochemical properties of nitrogen-doped TiO_2, J. Phys. Chem. B 108 (2004) 19384–19387.
[25] M. Miyauchi, A. Ikezawa, H. Tobimatsu, H. Irie, K. Hashimoto, Zeta potential and photocatalytic activity of nitrogen doped TiO_2 thin films, Phys. Chem. Chem. Phys. 6 (2004) 865–870.
[26] E. Barraud, F. Bosc, D. Edwards, N. Keller, V. Keller, Gas phase photocatalytic removal of toluene effluents on sulfated titania, J. Catal. 235 (2005) 318–326.
[27] V. Keller, P. Bernhardt, F. Garin, Photocatalytic oxidation of butyl acetate in vapor phase on TiO_2, Pt/TiO_2 and WO_3/TiO_2 catalysts, J. Catal. 215 (2003) 129–138.
[28] T. Klimnova, E. Carmona, J. Ramirez, Organic polymers as pore-regulating agents in TiO_2–Al_2O_3 mixed oxide catalytic supports, J. Mater. Sci. 33 (1998) 1981.
[29] O. Rosseler, M.V. Shankar, M. Karkmaz-Le Du, L. Schmidlin, N. Keller, V. Keller, Solar light photocatalytic hydrogen production from water over Pt and Au/TiO_2 (anatase/rutile) photocatalysts: influence of noble metal and porogen promotion, J. Catal. 269 (2010) 179–190.
[30] N.L. Wu, S.Y. Wang, J.A. Rasukova, Inhibition of crystallite growth in the sol–gel synthesis of nanocrystalline metal oxides, Science 285 (1999) 1375–1377.
[31] C.M. Jin, J.D. Luttmer, D.M. Smith, T.A. Ramos, Nanoporous silica as an ultralow-k dielectric, Mater. Res. Soc. Bull. 22 (10) (1997) 39–42.
[32] N. Keller, E. Barraud, F. Bosc, D. Edwards, V. Keller, On the modification of photocatalysts for improving visible light an UV degradation of gas-phase toluene over TiO_2, Appl. Catal. B: Environ. 70 (2007) 423–430.

[33] M. Grandcolas, M. Karkmaz-Le Du, F. Bosc, A. Louvet, N. Keller, V. Keller, Porogen template assisted TiO_2 rutile coupled nanomaterials for improved visible and solar light photocatalytic applications, Catal. Lett. 123 (2008) 65–71.
[34] J.M. Herrmann, Heterogeneous photocatalysis: state of the art and present applications, Top. Catal. 34 (1–4) (2005) 49–65.
[35] C. Wu, Y. Yue, X. Deng, W. Hua, Z. Gao, Investigation on the synergetic effect between anatase and rutile nanoparticles in gas-phase photocatalytic oxidations, Catal. Today 93–95 (2004) 863–869.
[36] H. Uchida, S. Itoh, H. Yoneyama, Photocatalytic decomposition of propyzamide using TiO_2 supported on activated carbon, Chem. Lett. 22 (1993) 1995.
[37] S. Nottakun, J.C. Crittenden, D.W. Hand, D.L. Perram, M.E. Mullins, Regeneration of adsorbents using heterogeneous advanced oxidation, J. Environ. Eng. 119 (1993) 695–714.
[38] S. Sampath, H. Uchida, H. Yoneyama, Photocatalytic degradation of gaseous pyridine over zeolite-supported titanium dioxide, J. Catal. 149 (1994) 189–194.
[39] Y. Xu, C.H. Langford, Enhanced photoactivity of a titanium(IV) oxide supported on ZSM5 and zeolite A at low coverage, J. Phys. Chem. 99 (29) (1995) 11501–11507.
[40] C. Anderson, A. Bard, An improved photocatalyst of TiO_2/SiO_2 prepared by a sol–gel synthesis, J. Phys. Chem. 99 (24) (1995) 9882–9885.
[41] T. Tatsuma, S. Tachibana, A. Fujishima, Remote oxidation of organic compounds by UV-irradiated TiO_2 via the gas phase, J. Phys. Chem. B 105 (29) (2001) 6987–6992.
[42] H. Haick, Y. Paz, Remote photocatalytic activity as probed by measuring the degradation of self-assembled monolayers anchored near microdomains of titanium dioxide, J. Phys. Chem. B 105 (15) (2001) 3045–3051.
[43] M.C. Lee, W. Choi, Solid phase photocatalytic reaction on the soot/TiO_2 interface: the role of migrating OH radicals, J. Phys. Chem. B 106 (45) (2002) 11818–11822.